Room Temperature Synthesis of Lead-Free Sn/Ge-Based Perovskite Quantum Dots

Zeying Chen[1,3], Pravakar P. Rajbhandari[1,2], and Tara P. Dhakal[1-3]

[1]Center for Autonomous Solar Power (CASP), [2]Department of Electrical and Computer Engineering, and [3]Material Science and Engineering Program, Binghamton University, Binghamton, NY 13902, USA

***Abstract* — Metal halide perovskites have received remarkable attention as photovoltaic (PV) devices. These have already achieved power conversion efficiency higher than 23% rivaling that of silicon-based PV. However, these outstanding efficiencies can only be acquired with lead-based perovskites and the devices are chemically unstable in air and moisture. Therefore, the key to the widespread deployment of perovskite-based solar cell will come down to address their "toxicity" and instability problems. We have taken the challenge to replace lead with other nontoxic or less toxic elements, e.g., Sn, and Ge. We have synthesized Cs(Sn,Ge)X_3 (X=I, Br, and Cl) quantum dots (QDs) using room temperature process. The XRD data showed that the synthesized QDs were yellow hexagonal phase, which was further confirmed by the hexagonal shape of the TEM images of the crystals.**

***Index Terms* — Lead-free perovskite, nanoparticle, doping photoluminescence, solar cell.**

I. Introduction

In recent years, halide perovskite quantum dots (QDs) have become the rising star of optoelectronics semiconductor materials for applications such as solar cell, light emitting diodes, photodetectors, etc. Halide perovskite is an absorber material in solar cell that showed a great improvement of power conversion efficiency (PCE) from 3.81% to now approaching 24% within ten years [1], rivaling PCE (27%) of silicon-based solar cells that was achieved through 30 years of effort. This outstanding performance is achieved based on the unique optoelectronic properties of the halide perovskite, such as high charge carrier mobilities ($25\,cm^2/Vs$), long carrier diffusion length (>1μm) [2], high absorption coefficients, and direct and tunable band gap. Moreover, low-cost perovskite quantum dots can be synthesized through earth-abundant materials including alkaline earth metal and lanthanide-based materials [3], which demanded more attention.

The general chemical formula of metal halide perovskites is ABX_3, where A =$CHNH^+$, $HC(NH)^+$, Cs^+, etc., B = Pb, Sn, and Ge; and X = Cl, Br, and I. The state-of-the-art perovskite solar cells use lead-based perovskite absorber. The toxicity of lead is a serious hurdle for the widespread commercialization of perovskite solar cell technology. Thus, a great effort is being devoted to the synthesis of low-cost, high efficiency and "lead-free" perovskite. Several lead-free elements have been proposed in halide perovskite, such as Ge (II) [4], Sn (II) [5], Bi (III) [6], Sb (III) [7], Ti (IV) [8], and Ag (I) [9]. Among them, Sn-based perovskites, including $CH_3NH_3SnI_3$, $HC(NH_2)_2SnI_3$, and $CsSnI_3$ are promising because of their lower bandgap and corresponding reasonable device performance. While $CH_3NH_3SnI_3$, and $HC(NH_2)_2SnI_3$ have PCEs up to 9% [10], their stability is low, which is not only attributed to the oxidation of Sn^{2+} but also to the organic cations volatilization [10]. Consequently, all inorganic lead-free perovskites have been explored. The inorganic lead-free perovskite based on Sn such as $CsSnI_3$ has recently achieved a PCE of 5% [11].

Herein, we take up the challenge to partially or fully replace Sn with Ge following the ligand-assisted re-precipitation (LARP) method [12], which has not been applied on the synthesis of lead-free perovskite. The synthesis is carried out at room temperature.

II. Experiment

Colloidal $CsSn(Br_xI_{1-x})_3$ (x=0, 0.2, 0.25, 0.5, 1) nanocrystals were fabricated by following LARP method in the N_2 filled glove box at room temperature. It is accomplished by transferring precursor solution of SnX_2 (X=Br, I) and CsX dissolved in a good solvent N, N-dimethylformamide (DMF) into vigorously stirred poor solvent toluene together with a ligand trioctylphosphine (TOP). Due to the huge difference in solubility of perovskite in DMF and in toluene, precursors get crystalized in toluene and form colloidal nanoparticles.

Furthermore, in order to investigate if partially tuning A-site and B-site cation composition in perovskite helps stabilizing the perovskite structure of $CsSnX_3$, substitution of Cs with larger formamidinium (FA) cation in $CsSnI_3$ was carried out. In addition, substitution of Ge into Sn-site in $CsSnBr_3$ and $CsSnBr_{1.5}I_{1.5}$ were conducted.

A. Synthesis of $CsSn(Br_xI_{1-x})_3$ (x=0, 0.2, 0.25, 0.5, 1)

In a typical synthesis of $CsSnBr_3$ a mixture of 0.105 mmol $SnBr_2$, and 0.105 mmol CsBr were dissolved in 2.6 ml DMF, which functions as good solvent that dissolve the inorganic salt and small molecules and form a clear precursor solution [12]. 0.435 mL of precursor solution was transferred dropwise into 5 mL "poor" solvent toluene with vigorous stirring. Along with the mixing, the white-yellow solution was obtained and started to glow green-yellow, which indicated the formation of colloidal nanoparticles. After that, 10 μL of TOP added to stop the growth.

$CsSnI_3$ and $CsSn(Br_xI_{1-x})_3$ were obtained by adjusting the amount of precursors and following the same LARP method.

978-1-7281-0494-2/19/$31.00 ©2019 IEEE

B. Syntheses of $Cs_{1-x}FA_xSn(Br_xI_{1-x})_3$, $CsSn_{1-x}Ge_xBr_3$, and $CsSn_{1-0.5x}Ge_{0.5x}Br_{1.5}I_{1.5}$

$Cs_{1-x}FA_xSn(Br_xI_{1-x})_3$ (x = 5%, 10%, 15%, 20%, 35%, 50%), $CsSn_{1-x}Ge_xBr_3$ (x = 3%, 6%, 9%) and $CsSn_{1-0.5x}Ge_{0.5x}Br_{1.5}I_{1.5}$ (x= 10%, 20%, 30%, 50%) were all prepared by following LARP method and the Cs, and Sn composition ratios were respectively tuned in each perovskite structure.

C. Characterizations

The photoluminescence characteristics of all of samples were obtained using Horiba's PL measurement system with mono-chromated xenon lamp source of 370 nm excitation and photo multiplier tube (PMT) detector. The crystallographic characterization is performed with X-ray diffraction (XRD) using Pan-Analytical X-Pert PRO X-ray diffraction system which used CuKα X-ray and line-focus optics. It is performed in ambient air after spin coating with PCBM (Phenyl C60 butyric acid methyl ester) on top of QDs to prevent short term degradation. The size and shape of particles were indicated by Transmission electron microscope (TEM).

III. Analysis

A. $CsSn(Br_xI_{1-x})_3$ (x=0, 0.2, 0.5, 0.8, 1) Synthesized by LARP Methods

The LARP technique could be conveniently employed to synthesize $CsSn(Br_xI_{1-x})_3$ (x=0, 0.2, 0.5, 0.8, 1) by tuning halide substitutions. Fig.1 shows the optical images of $CsSn(Br_xI_{1-x})_3$ samples under 365 nm UV light, and all of them were fluorescing. In Fig. 2, the PL spectra ranged from 518 nm for $CsSnBr_3$, to 578 nm for $CsSnBr_{1.5}I_{1.5}$ by adjusting the composition of halogen. Since Sn-based perovskite nanoparticles exhibit poor stability even under the protection of long-chain ligand, the purification process was not carried out at this time. The FWHM were about 100 nm resulting from the absence of purification process.

In contrast to expectations, for compositions of iodine more than 50%, $CsSn(Br_xI_{1-x})_3$ did not exhibit further red shift than that of $CsSn(Br_{0.5}I_{0.5})_3$. The glow was more toward yellow-orange, exhibiting a blue shift. $CsSnI_3$ is reported having two orthorhombic polymorphs at room temperature [13]. One is black orthorhombic phase (B-γ) having 3D perovskite structure with a direct band gap of 1.3 eV. The other is yellow phase (Y), which has 1D double-chain structure and indirect band gap of 2.55 eV, which is not desirable. Yellow phase (Y) is thermodynamically stable at room temperature. Comparing with yellow phase, B-γ is kinetically stabilized metastable phase, which convert to yellow phase when contact with humidity, oxygen, change of pressure, etc. In our results, the accidental blue shift might be led by easy phase transition from black phase of ABI_3 to yellow phase. In Fig. 3(a), the labeled XRD spectra of $CsSnBr_{1.5}I_{1.5}$ is in agreement with the yellow and B-γ phase reported by Kontos et.al.[13]. The first peak located at 25.87° might exhibit a coexistence of yellow and B-γ phase peak because of its broadness. The Y and B-γ phase peaks in our case showed slight right shift in position comparing with the reference [13]. This is because the XRD peaks of yellow and B-γ phase provided by Kontos et al. [13] were based on $CsSnI_3$, whereas in our case, it was a slightly different composition, $CsSnBr_{1.5}I_{1.5}$. As I ion was partially replaced by Br ion in $CsSnX_3$ structure, lattice parameter decreases resulting in a right shift in angle.

Besides, TEM image (Fig. 3(b)) indicated the shape of orthorhombic yellow or black phase $CsSnBr_{1.5}I_{1.5}$ perovskite that is covered by ligand. The post-synthesis purification leads the detachment of partial ligand from particles as well as the dispersion of particles. As a result, we were not able to acquire the accurate particle size by TEM due to the inability of purification process. The size was in the range of 20-40 nm.

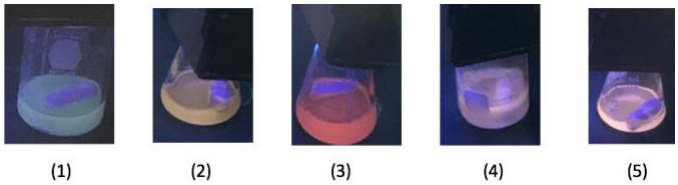

Fig. 1. Optical images of $CsSn(Br_xI_{1-x})_3$ under UV light (365 nm). Nos.1-5 are $CsSnBr_3$, $CsSnBr_{2.4}I_{0.6}$, $CsSnBr_{1.5}I_{1.5}$, $CsSnBr_{0.6}I_{2.4}$, and $CsSnI_3$ respectively.

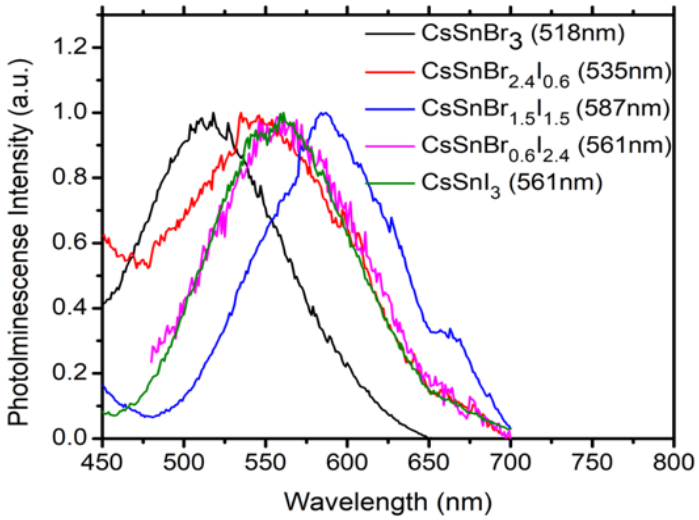

Fig. 2. Normalized PL emission spectra of $CsSn(Br_xI_{1-x})_3$ and their respective peak position.

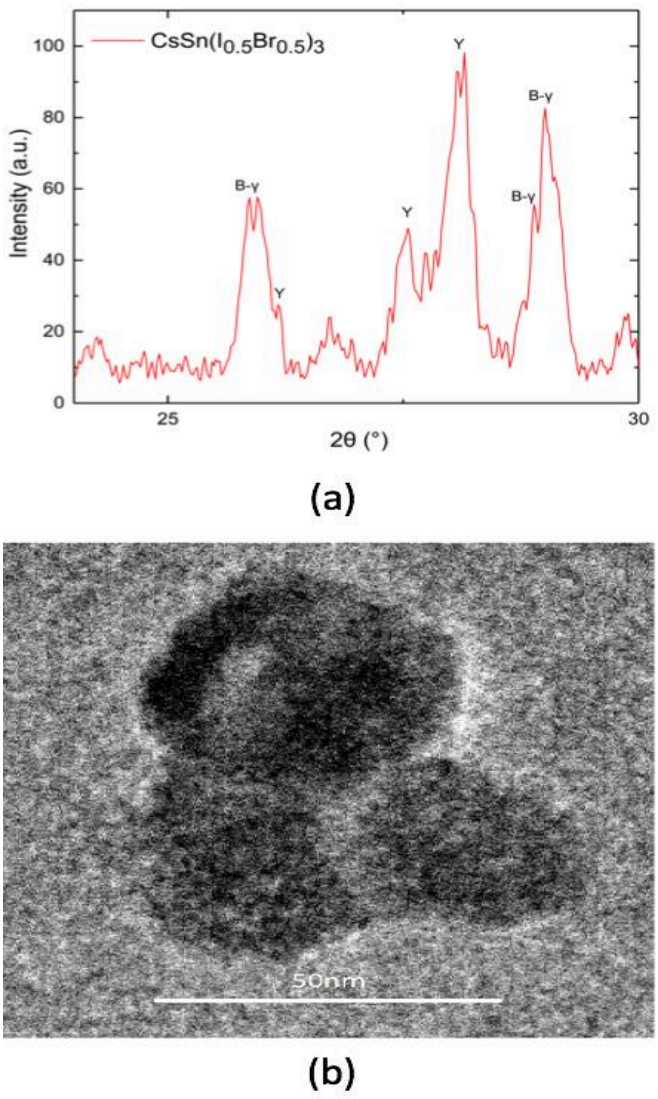

Fig. 3. (a) XRD image (Y: yellow phase, B-γ: black gamma phase) and (b) TEM of $CsSnBr_{1.5}I_{1.5}$.

B. Substitution of Cs with FA

In order to help $CsSnI_3$ form an optimal phase, mixing FA with Cs was conducted. Replacing A-site cation with bigger ion, such as FA, might be helpful for stabilizing the α-phase of I-based perovskites as well as regulate phase transformation [14]. As shown in Fig. 4, the substitution of Cs with bigger FA cation led to a blue-shift and a slight increase in the photoluminescence intensity. For lead-based halide perovskite, the substitution of smaller Cs cation with FA leads to the decrease in band gap resulting from BX_6 octahedral tilting. It has been confirmed by both computational and experimental results of lead-based perovskite [15]. The change in band gap of $Cs_{1-x}FA_xSn(Br_xI_{1-x})_3$ (x=5% to 50%) was in accordance with the trend of Pb-based perovskite. Moreover, the proper ratio of A-site alloying improved PL performance.

However, the addition of FA did not contribute to the right phase transition, which might result from the absence of other conditions that have to be satisfied, such as temperature, right solvent and ligand.

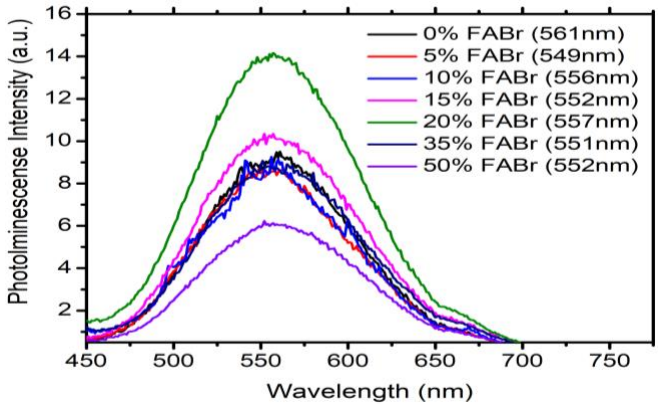

Fig. 4. PL emission spectra of mixed $Cs_{1-x}FA_xSn(Br_xI_{1-x})_3$ and their respective peak position.

C. Mixed Ge-Sn Perovskite

By incorporating $GeBr_2$ from 5% to 50%, the PL peak of $CsSnBr_{1.5}I_{1.5}$ slightly blue-shifted from 587 nm or remained similar (Fig. 5). In Chi et al. [16] research, GeI_2 was confirmed to reduce the trap densities in $FA_{0.75}MA_{0.25}SnI_3$ perovskite structure resulting in a slight blue shift from 919 nm to 914 nm. Further investigation will be carried out to find the detailed reason for blue shift.

In Fig.6, the addition of $GeBr_2$ in $CsSnBr_3$ didn't lead to any obvious change in bandgap. However, for both $CsSnBr_3$ and $CsSnBr_{1.5}I_{1.5}$, the addition of Ge gave rise to the unexpected decrease in PL intensity.

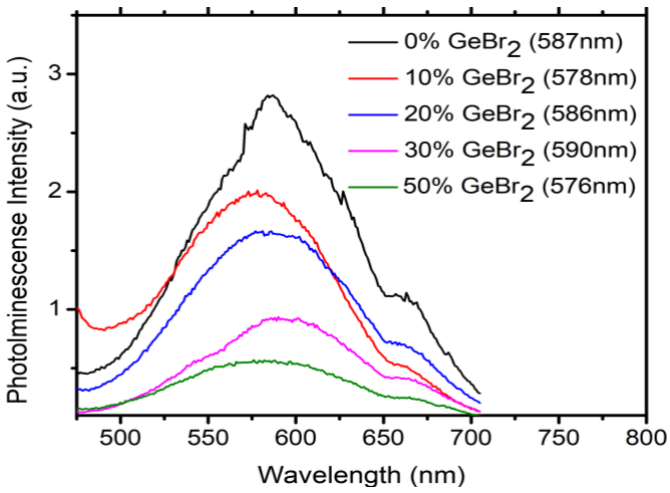

Fig. 5. Emission spectra of $CsSn_{1-0.5x}Ge_{0.5x}Br_{1.5}I_{1.5}$ and their respective peak position.

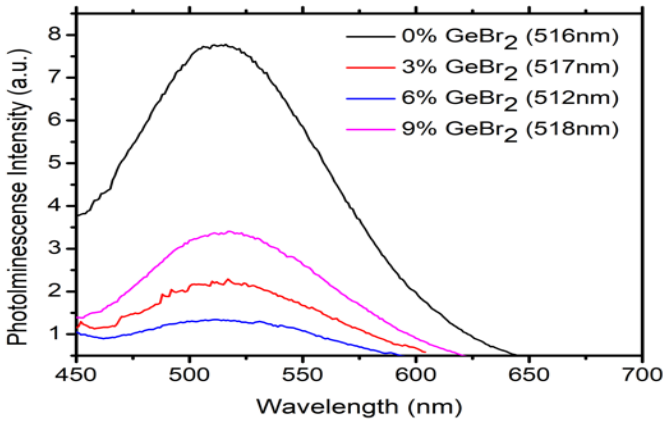

Fig. 6. PL emission spectra of $CsSn_{1-x}Ge_xBr_3$ and their respective peak position.

IV. Summary

A more convenient method than hot-injection method, LARP technique, was firstly demonstrated on the synthesis of Sn-based perovskite, which realized the formation of $CsSn(Br_xI_{1-x})_3$ at room temperature by simply tuning composition of halogen. In this study, the band gap was tuned from 518 nm to 587 nm as Br in perovskite structure was partially replaced by I ion. Even with further addition of I (>50%), PL spectra did not show a continuous red shift, which resulted from the formation of yellow phase. However, even for this room temperature synthesis, a reasonable fluorescence performance was observed. Ge was substituted in several $CsSnBr_3$ and $CsSnBr_{1.5}I_{1.5}$ compositions resulted in slight blue shift and reduced PL intensities. A slight blue-shift and increase in photoluminescence intensity were observed in FA alloyed $CsSnI_3$. The decrease in band gap might be due to BX_6 octahedral tilting as bigger cation added, which follows the similar trend in the band gap of Cs-FA mixed lead-base perovskite. Besides, the proper ratio of FABr alloying improved the PL performance. More work will be done to form and stabilize Sn/Ge based perovskite into black phase. LARP method will be further modified to synthesize the Ge-substituted $CsSnI_3$ in an optimal perovskite structure.

References

[1] Jeon, N. J., Na, H., Jung, E. H., Yang, T. Y., Lee, Y. G., Kim, G., Shin, H. & Seo, J. (2018). A fluorene-terminated hole-transporting material for highly efficient and stable perovskite solar cells. Nature Energy, 3(8), 682.

[2] Chen, Q., De Marco, N., Yang, Y. M., Song, T. B., Chen, C. C., Zhao, H., Hong, Z., Zhou, H. & Yang, Y. (2015). Under the spotlight: The organic–inorganic hybrid halide perovskite for optoelectronic applications. Nano Today, 10(3), 355-396.

[3] Kieslich, G., Sun, S., & Cheetham, A. K. (2015). An extended tolerance factor approach for organic–inorganic perovskites. Chemical science, 6(6), 3430-3433.

[4] Krishnamoorthy, T., Ding, H., Yan, C., Leong, W. L., Baikie, T., Zhang, Z., Sherburne, M., Li, S., Asta, M., Mathews, N., & Mhaisalkar, S. G. (2015). Lead-free germanium iodide perovskite materials for photovoltaic applications. Journal of Materials Chemistry A, 3(47), 23829-23832.

[5] Wang, N., Zhou, Y., Ju, M. G., Garces, H. F., Ding, T., Pang, S., Zeng, X. C., Padture, N. P. & Sun, X. W. (2016). Heterojunction-Depleted Lead-Free Perovskite Solar Cells with Coarse-Grained B-γ-CsSnI3 Thin Films. Advanced Energy Materials, 6(24), 1601130.

[6] Zhang, Z., Li, X., Xia, X., Wang, Z., Huang, Z., Lei, B., & Gao, Y. (2017). High-quality (CH3NH3) 3Bi2I9 film-based solar cells: pushing efficiency up to 1.64%. The journal of physical chemistry letters, 8(17), 4300-4307.

[7] Zuo, C., & Ding, L. (2017). Lead-free Perovskite Materials (NH4) 3Sb2IxBr9− x. Angewandte Chemie International Edition, 56(23), 6528-6532.

[8] Chen, M., Ju, M. G., Carl, A. D., Zong, Y., Grimm, R. L., Gu, J., Zeng, X. C., Zhou, Y., & Padture, N. P. (2018). Cesium titanium (IV) bromide thin films based stable lead-free perovskite solar cells. Joule, 2(3), 558-570.

[9] Du, K. Z., Meng, W., Wang, X., Yan, Y., & Mitzi, D. B. (2017). Bandgap Engineering of Lead-Free Double Perovskite Cs2AgBiBr6 through Trivalent Metal Alloying. Angewandte Chemie International Edition, 56(28), 8158-8162.

[10] Chen, M., Ju, M. G., Garces, H. F., Carl, A. D., Ono, L. K., Hawash, Z., Zhang, Y., Shen, T., Qi, Y., Grimm, R. L., Zeng, X. C., & Pacifici, D. (2019). Highly stable and efficient all-inorganic lead-free perovskite solar cells with native-oxide passivation. Nature communications, 10(1), 16.

[11] Wang, Y., Tu, J., Li, T., Tao, C., Deng, X., & Li, Z. (2019). Convenient preparation of CsSnI 3 quantum dots, excellent stability, and the highest performance of lead-free inorganic perovskite solar cells so far. Journal of Materials Chemistry A.

[12] Zhang, F., Zhong, H., Chen, C., Wu, X. G., Hu, X., Huang, H., Han, J., Zou, B., & Dong, Y. (2015). Brightly luminescent and color-tunable colloidal CH3NH3PbX3 (X= Br, I, Cl) quantum dots: potential alternatives for display technology. ACS nano, 9(4), 4533-4542.

[13] Kontos, A. G., Kaltzoglou, A., Siranidi, E., Palles, D., Angeli, G. K., Arfanis, M. K., Psycharis, V., Raptis, Y. S., Kamitsos, E. I., Thikalitis, P. N., & Stoumpos, C. C. (2016). Structural stability, vibrational properties, and photoluminescence in CsSnI3 perovskite upon the addition of SnF2. Inorganic chemistry, 56(1), 84-91.

[14] Xu, L., Yuan, S., Zeng, H., & Song, J. (2019). A comprehensive review of doping in perovskite nanocrystals/quantum dots: evolution of structure, electronics, optics and light-emitting diodes. Materials Today Nano, 100036.

[15] Prasanna, R., Gold-Parker, A., Leijtens, T., Conings, B., Babayigit, A., Boyen, H. G., Toney, M. F., & McGehee, M. D. (2017). Band gap tuning via lattice contraction and octahedral tilting in perovskite materials for photovoltaics. Journal of the American Chemical Society, 139(32), 11117-11124.

[16] Ng, C. H., Nishimura, K., Ito, N., Hamada, K., Hirotani, D., Wang, Z., Yang, F., Likubo, S., Shen, Q., Yoshino, K., Minemoto, T & Hayase, S. (2019). Role of GeI2 and SnF2 additives for SnGe perovskite solar cells. Nano Energy, 58, 130-137.